Fitting Concentric Elliptical Shapes Under General Model

Ali Al-Sharadqah[1*] and Giuliano Piga[1]

[1*]Department of Mathematics and Interdisciplinary Research Institute for the Sciences, IRIS, California State University, 18111 Nordhoff Street, Northridge, 91330, CA, US.

*Corresponding author(s). E-mail(s): ali.alsharadqah@csun.edu;
Contributing authors: giuliano.piga.42@my.csun.edu;

Abstract

The problem of fitting concentric ellipses is a vital problem in image processing, pattern recognition, and astronomy. Several methods have been developed but all address very special cases. In this paper, this problem has been investigated under a more general setting, and two estimators for estimating the parameters have been proposed. Since both estimators are obtained iterative fashion, several numerical schemes are investigated and the best initial guess is determined. Furthermore, the constraint Cramé Rao lower bound for this problem is derived and it is compared with the variance of each estimator. Finally, our theory is assessed and validated by a series of numerical experiments on both real and synthetic data.

Keywords: concentric ellipses, error analysis, constraint Cramér Rao lower bound, iterative methods

1 Introduction

Computer vision is a broad field with a host of data-centric challenges to be addressed. One such class of challenges, for example, is image recognition problems, in which an image is to be classified as belonging to a class of images or not. Image recognition problems are often handled with generalized methods, such as convolutional neural networks Aggarwal (2018). The methods used to solve these problems are often robust but are not designed for a specific type of data. Data-specific models can be used when more than classification is of interest. For example, if an object is known (or assumed) to belong to a certain class of objects, one might be interested in its dimensions, or some parameters of its underlying shape, given an image of it. These sorts of problems are handled are known as *Geometric Estimation*, which plays a vital role in computer vision and medical imaging Bennamoun and Mamic (2002); Kanatani and Sugaya (2016); Zhao and Xiong (2011), petroleum engineering M. Heidari (1993); Kilambi et al (2011), astronomy Ambartsoumian and Xie (2010), bioinformatics Kumar et al (2018), object classifications S. D. Connell (2001), and many other fields.

In this paper, we will discuss a special problem in geometric fitting, namely, concentric ellipse fitting. This has been an active research area recently because of its applications in camera calibration Kweon et al (2002), and biometrics and iris recognition Al-Sharadqah and Rulli (2022). Moreover, it has tremendous applications in astronomy Salo and et al (2014) and engineering Kanatani (2008). Ellipses are a commonly occurring shape in nature, especially since the projection of circular objects into the image plane is elliptical. This has made the problem of ellipse fitting popular among researchers and engineers Chang and Weiduo (2019); Al-Sharadqah and Chernov (2012); Chang and Weiduo (2019); Taubin (1991) and much more. Several methods, such as the *Maximum*

Likelihood Estimation method (MLE) or *Orthogonal Distance Regression* have proven to provide the best estimates of the ellipse parameters. These methods, however, pose a major drawback, being the computational time required to obtain those estimates. Alternatively, cheaper but less accurate methods, such as, the *algebraic methods* were developed. This paper focuses on fitting concentric ellipses where we develop methods that provide accurate estimates of the parameters and we will establish their Cramér Rao lower bound. We will also show which estimator has a variance that achieves this lower bound. It is worth mentioning here that whenever data is corrupted by outliers those approaches fail, and as such other approaches such as RANSAC or its variant shall be used Mai et al (2008); Vincze (2001); Satriya et al (2016).

Along these lines, Al-Sharadqah and Rulli (2022) study the problem of concentric ellipse fitting under some restrictive constraints where they assume that the tilt angles of the concentric ellipses are equal and also the major and the minor axis lengths of the two ellipses are proportional (i.e. if Ellipse 1 has major and minor axes a_1 and b_1 and Ellipse 2 has major and minor axes a_2 and b_2, then $\frac{a_1}{b_1} = \frac{a_2}{b_2}$). This allows them to represent the problem algebraically and develop several non-iterative methods. However, imposing those constraints adds limitations to their practical uses in real-life applications. For example, one might be interested in identifying the structure of galaxies Salo and et al (2014) by estimating the mass-to-luminosity ratio of nearby galaxies. In this case, the algorithm of Al-Sharadqah and Rulli (2022) is not applicable, and as such, new models are needed to handle this general case. Therefore, we will relax their assumption in this paper and we will only assume that the data are perturbed digitized pixels coming from any concentric ellipses.

To formulate this problem mathematically, let us first assume the observations $\boldsymbol{m}_{ij} = (x_{ij}, y_{ij})^\top$, $i \in \{1, 2, \ldots, k\}$, $j \in \{1, \ldots, n_i\}$ coming from k

concentric ellipses. The point $\boldsymbol{m}_{ij}$ is the j^{th} point of the i^{th} ellipse. We also assume that the observation $\boldsymbol{m}_{ij}$ is a noisy point of a true (but unknown) point $\tilde{\boldsymbol{m}}_{ij} = (\tilde{x}_{ij}, \tilde{y}_{ij})$ that lies exactly on the i^{th} ellipse, and as such, it satisfies

$$\mathcal{P}(\tilde{\boldsymbol{m}}_{ij}, \tilde{\boldsymbol{\theta}}) = 0, \tag{1}$$

where

$$\mathcal{P}(\tilde{\boldsymbol{m}}_{ij}, \tilde{\boldsymbol{\theta}}) = \frac{\tilde{T}^2}{\tilde{a}_i^2} + \frac{\tilde{T}_{ij}'^2}{\tilde{b}_i^2} - 1 := \tilde{p}_{ij} \quad \text{(say)}, \tag{2}$$

and

$$\begin{aligned} \tilde{T}_{ij} &= \big(\tilde{x}_{ij} - \tilde{x}_c\big)\cos(\tilde{\psi}_i) + \big(\tilde{y}_{ij} - \tilde{y}_c\big)\sin(\tilde{\psi}_i) \\ \tilde{T}'_{ij} &= -\big(\tilde{x}_{ij} - \tilde{x}_c\big)\sin(\tilde{\psi}_i) + \big(\tilde{y}_{ij} - \tilde{y}_c\big)\cos(\tilde{\psi}_i). \end{aligned} \tag{3}$$

Here $\tilde{x}_c$ and $\tilde{y}_c$ stand for the coordinates for the common center of the concentric ellipses, while the parameters $\tilde{a}_i$'s and $\tilde{b}_i$'s are the major and minor axis lengths, respectively, and $\tilde{\psi}_i$'s represent the tilt angles. The vectors of parameters $\tilde{\boldsymbol{\theta}} = (\tilde{x}_c, \tilde{y}_c, \tilde{a}_1, \tilde{b}_1, \tilde{\psi}_1, \ldots, \tilde{a}_k, \tilde{b}_k, \tilde{\psi}_k)^\top$ is unknown and shall be estimated. Accordingly, we will assume the additive-measurement error model, i.e., $\boldsymbol{m}_{ij} = (x_{ij}, y_{ij})^\top$ are perturbed from their true points as $\boldsymbol{m}_{ij} = \tilde{\boldsymbol{m}}_{ij} + \boldsymbol{n}_{ij}$, where $\boldsymbol{n}_{ij} = (\delta_{ij}, \epsilon_{ij})^\top$ is a noisy vector. Due to this, the stochastic nature of the observations makes this research problem falls under *Errors-In-Variables (EIV) Models*. In EIV models, the statistical nature of the true point is crucial: If the points are regarded as fixed but unknown, the model is called a *functional model*. If the points are stochastic, the model is called a *structural model*. In this paper, we adopt the functional model as it is more natural in computer vision and image processing applications.

This paper is organized as follows. In Section 2 we propose two methods to estimate the parameters. In Section 3, we derive the Constraint Cramér Rao Lower Bound. Section 4 introduces more statistical assumptions and studies the statistical properties of both estimators. In Section 5 we develop estimators for σ^2. In Section 6, we describe the numerical implementation for the two methods and propose a good initial guess and we also validate the theory through a series of numerical experiments on both real and synthetic data.

2 Methods

In order to estimate $\boldsymbol{\theta}$, we will implement two approaches: the Least Squares (LS) and the Gradient weighted Algebraic Fit (GRAF). The LS minimizes

$$\mathcal{F}_{\mathrm{L}}(\boldsymbol{\theta}) = \sum_{i=1}^{k} \sum_{j=1}^{n_i} p_{ij}^2, \tag{4}$$

while The GRAF minimizes

$$\mathcal{F}_{\mathrm{G}}(\boldsymbol{\theta}) = \sum_{i=1}^{k} \sum_{j=1}^{n_i} \frac{p_{ij}^2}{\|\nabla p_{ij}\|^2}, \tag{5}$$

where $\nabla p_{ij} = \frac{\partial p_{ij}}{\partial \boldsymbol{m}_{ij}}$. The GRAF is an approximation of the MLE and it minimizes the weighted sum of the squares of the algebraic distances p_{ij}.

In the problem of fitting all other primitive geometric shapes, such as circles, ellipses, and concentric ellipses (under the Al-Sharadqah and Rulli model), the LS is a non-iterative method that is easy to compute. However, under our general model, the situation is different. Here $\mathcal{P}(\boldsymbol{m}_{ij}, \boldsymbol{\theta})$ is a highly non-linear function, which makes the minimization process of $\mathcal{F}$ not easy to deal with. The reason here is that it is infeasible to linearize $\mathcal{P}$. As a remedy, we propose to 'partially linearize' (4) with a new parameter vector $\boldsymbol{\phi}$ as

$\boldsymbol{\phi} = (x_c, y_c, A_1, B_1, \psi_1, \ldots, A_k, B_k, \psi_k)^\top$, where $A_i = \frac{1}{a_i^2}$ and $B_i = \frac{1}{b_i^2}$, for $i = 1, \ldots, k$. After $\boldsymbol{\phi}$ is estimated, the geometric parameter vector $\boldsymbol{\theta}$ can be retrieved. Here we will denote by $\hat{\boldsymbol{\phi}}_{\mathrm{L}}$ and $\hat{\boldsymbol{\phi}}_{\mathrm{G}}$ the LS and the GRAF estimates by, respectively, which minimize $\mathcal{F}_{\mathrm{L}}(\boldsymbol{\phi})$ and $\mathcal{F}_{\mathrm{G}}(\boldsymbol{\phi})$, respectively; i.e.

$$\hat{\boldsymbol{\phi}}_{\mathrm{L}} = \mathrm{argmin}_{\boldsymbol{\phi}} \mathcal{F}_{\mathrm{L}}(\boldsymbol{\phi}) = \mathrm{argmin}_{\boldsymbol{\phi}} \sum_{i=1}^{k} \sum_{j=1}^{n_i} p_{ij}^2. \tag{6}$$

and

$$\hat{\boldsymbol{\phi}}_{\mathrm{G}} = \mathrm{argmin}_{\boldsymbol{\phi}} \mathcal{F}_{\mathrm{G}}(\boldsymbol{\phi}) = \mathrm{argmin}_{\boldsymbol{\phi}} \sum_{i=1}^{k} \sum_{j=1}^{n_i} \frac{p_{ij}^2}{\|\nabla p_{ij}\|^2}, \tag{7}$$

where $\nabla p_{ij} = \frac{\partial p_{ij}}{\partial \boldsymbol{m}_{ij}} = 2(T_{ij} A_i C_i - T'_{ij} B_i S_i, T_{ij} A_i S_i + T'_{ij} B_i C_i)^\top$. Here we define $C_i = \cos(\psi_i)$ and $S_i = \sin(\psi_i)$ for $i = 1, \ldots, k$. Both objective functions are nonlinear and numerical methods as shall be implemented as shown in Section 6.

3 Constraint Cramèr-Rao Lower Bound

We would like to compare the accuracy of the two estimators to a theoretical accuracy limit, and as such, we know how good an estimator can actually be. In traditional statistics, the efficiency of any unbiased estimator can be determined by the *Cramèr Rao lower bound* (CRB): the variance (covariance matrix) $\boldsymbol{V}$ of an unbiased estimator satisfying $\boldsymbol{V} \geq \boldsymbol{D}_{\min}$ in the sense that $\boldsymbol{V} - \boldsymbol{D}_{\min}$ is a positive semidefinite matrix, where $\boldsymbol{D}_{\min}$ is the inverse of the *Fisher Information Matrix* (FIM). Due to the complexity of the EIV model, there are virtually no known unbiased estimators because all the known ones are biased; so the classical CRB is not applicable. In computer vision and image processing, the parameters are often constrained, and then the FIM may not be invertible, so the derivation of the CRB becomes difficult.

Nonetheless, Kanatani (1998) derived a general form of the CRB in geometric estimation problem for any unbiased estimator, thus this result was, technically, vacuous. In passing all estimators in geometric estimation, which lies under the umbrella of EIV models, are biased. Chernov and Lesort (2004) realized that the Kanatani lower bound cannot be applied in all geometric estimation problems. Chernov and Lesort (2004) dealt with this drawback of the CRB by deriving the CRB with a minimal requirement called geometric consistency using error analysis. Chernov and Lesort (2004) used the Taylor expansion of the variance $\boldsymbol{V}$ (as the noise level $\sigma \to 0$) to prove that the *leading term* of $\boldsymbol{V}$ satisfies $\boldsymbol{V}_{\text{leading}} \geq \boldsymbol{D}_{\text{min}}$. Their bound applies to *all geometrically consistent estimators* as will be introduced in the next section. Chernov and Lesort employed first-order analysis of any geometrically consistent estimator to reach a lower bound on its variance. Up to the leading term, their lower bound coincides with the CRB of Kanatani, and as such, they call it the Katanani-Cramèr-Rao lower bound (or KCR for short), to recognizing the crucial contribution by Kanatani (1998). Now this name is adopted in the literature on the subject. Along these lines, Stoica and Ng (1998) derived a general form of the CRB for when there are constraints imposed on the parameter space assuming the estimator is unbiased and used their bound to some signal processing applications. Al-Sharadqah and Ho (2018) generalize the results of Stoica and Ng (1998) by relaxing the unbiasedness assumption. They also relax the assumption of orthogonality on $\boldsymbol{U}$ as stated in the following theorem. Before presenting the theorem and using it in our problem, we will elaborate a bit more on their lower bound.

In the functional model EIV models, the true points are fixed but unknown, and as such, they are considered nuisance parameters. Thus, if one is trying to fit a curve $P(\tilde{\boldsymbol{m}}, \tilde{\boldsymbol{\Theta}}) = 0$ to data, then this relation imposes constraints defined

by the true points and the true parameters. In our problem there are $n = \sum_{i=1}^{k} n_i$ constraints and $m = 2n + d$ parameters to estimate, where $d = 2 + 3k$. Thus, we will denote the bigger parameter space by $\tilde{\boldsymbol{\Theta}} = (\tilde{\boldsymbol{m}}^\top, \tilde{\boldsymbol{\phi}}^\top)^\top \in \mathbb{R}^m$, where $\tilde{\boldsymbol{m}} = (\tilde{\boldsymbol{m}}_{11}^\top, \ldots, \tilde{\boldsymbol{m}}_{1n_1}^\top, \ldots, \tilde{\boldsymbol{m}}_{k1}^\top, \ldots, \tilde{\boldsymbol{m}}_{kn_k}^\top)^\top \in \mathbb{R}^{2n}$ represents the combined vectors of all true points and $\tilde{\boldsymbol{\phi}} = (\tilde{x}_c, \tilde{y}_c, \tilde{A}_1, \tilde{B}_1, \tilde{\psi}_1, \ldots, \tilde{A}_k, \tilde{B}_k, \tilde{\psi}_k)^\top \in \mathbb{R}^d$ is the structural parameter vector. That is, $P_i(\tilde{\boldsymbol{m}}_{ij}, \tilde{\boldsymbol{\phi}}) = 0$, $j = 1 \ldots, n_i$, $i = 1, \ldots k$. impose $n-$constrains on the parameter space. In matrix notation, the model can be expressed as $\boldsymbol{P} = \boldsymbol{0}_{n\times 1}$, where $\boldsymbol{P} = (\tilde{p}_{11}, \ldots, \tilde{p}_{kn_k})^\top$ and $\tilde{p}_{ij} = \tilde{T}_{ij}^2 \tilde{A}_i + \tilde{T}_{ij}'^2 \tilde{B}_i - 1$. Since $\boldsymbol{P} = \boldsymbol{0}$ then there exists $\boldsymbol{U}_{m\times(m-n)}$ such that $\boldsymbol{F}_{n\times m}\boldsymbol{U} = \boldsymbol{0}_{n\times(m-n)}$ where $\boldsymbol{F} = \frac{\partial \boldsymbol{P}}{\partial \tilde{\boldsymbol{\Theta}}}$.Our goal here is to derive the Cramèr-Rao Lower Bound (CCRB) of $\tilde{\boldsymbol{\phi}}$ and possibly for the nuisance parameters $\tilde{\boldsymbol{m}}_i$'s. To accomplish this task, we will use the results of Al-Sharadqah and Ho (2018) to derive the CCRB of $\tilde{\boldsymbol{\Theta}}$. Then with some elements of linear algebra, we will derive the CCRB for our parameters of interest.

Let us first denote the Fisher Information Matrix (FIM) by $\boldsymbol{J} = \mathrm{E}(\boldsymbol{\Delta}\boldsymbol{\Delta}^\top)$, where $\boldsymbol{\Delta}$ is the score function of $\tilde{\boldsymbol{\Theta}}$, i.e., $\boldsymbol{\Delta} = \frac{\partial \log \mathcal{L}(\tilde{\boldsymbol{\Theta}})}{\partial \tilde{\boldsymbol{\Theta}}}$ and $\mathcal{L}(\tilde{\boldsymbol{\Theta}})$ is its likelihood function and assume the combined noise vector $\boldsymbol{n} = (\boldsymbol{n}_{11}^\top, \ldots, \boldsymbol{n}_{1n_1}^\top, \ldots, \boldsymbol{n}_{k1}^\top, \ldots, \boldsymbol{n}_{2n_k}^\top)_{2n\times 1}^\top$ is normally distributed with mean $\boldsymbol{0}_{2n}$ and positive definite variance-covariance matrix $\boldsymbol{\Sigma}_{2n}$. Next, we will use the following theorem.

Theorem 1 *(Al-Sharadqah and Ho (2018)) Let $\hat{\boldsymbol{\Theta}}$ be an estimator of $\tilde{\boldsymbol{\Theta}}$ satisfying some regularity conditions[1] and $\boldsymbol{J} = \mathbb{E}(\boldsymbol{\Delta}\boldsymbol{\Delta}^\top)$. Also, let $\boldsymbol{U}$ satisfy $\boldsymbol{F}\boldsymbol{U} = \boldsymbol{0}_{n\times(m-n)}$ with $\boldsymbol{U}$ spanning the null space of $\boldsymbol{F}$. Then if $\boldsymbol{U}^\top\boldsymbol{J}\boldsymbol{U}$ is nonsingular, then*

$$\mathrm{Cov}(\hat{\boldsymbol{\Theta}}) \geq \nabla_{\tilde{\boldsymbol{\Theta}}} \mathrm{E}(\hat{\boldsymbol{\Theta}}) \boldsymbol{U} (\boldsymbol{U}^\top \boldsymbol{J} \boldsymbol{U})^{-1} \boldsymbol{U}^\top \nabla_{\tilde{\boldsymbol{\Theta}}} \mathrm{E}(\hat{\boldsymbol{\Theta}})^\top. \tag{8}$$

[1]The regularity conditions are that the differential operator can be interchanged with the integral operator.

This lower bound applies to any problem as long as it satisfies the given assumptions. To apply this theorem here, we need to state our problem in the benchmark of this formulation. In particular

$$\begin{aligned}
\frac{\partial \tilde{p}_{ij}}{\partial \boldsymbol{m}_{ij}^{\top}} &= 2\left(\tilde{T}_{ij}\tilde{A}_i\tilde{C}_i - \tilde{T}'_{ij}\tilde{B}_i\tilde{S}_i, \tilde{T}_{ij}\tilde{A}_i\tilde{S}_i + \tilde{T}'_{ij}\tilde{B}_i\tilde{C}_i\right)\\
\frac{\partial \tilde{p}_{ij}}{\partial \tilde{x}_c} &= 2(\tilde{T}'_{ij}\tilde{B}_i\tilde{S}_i - \tilde{T}_{ij}\tilde{A}_i\tilde{C}_i)\\
\frac{\partial \tilde{p}_{ij}}{\partial \tilde{y}_c} &= -2(\tilde{T}'_{ij}\tilde{B}_i\tilde{C}_i + \tilde{T}_{ij}\tilde{A}_i\tilde{S}_i)\\
\frac{\partial \tilde{p}_{ij}}{\partial \tilde{A}_i} &= \tilde{T}^2_{ij}\\
\frac{\partial \tilde{p}_{ij}}{\partial \tilde{B}_i} &= \tilde{T}'^2_{ij}\\
\frac{\partial \tilde{p}_{ij}}{\partial \tilde{\psi}_i} &= 2(\tilde{T}_{ij}\tilde{T}'_{ij}\tilde{A}_i - \tilde{T}_{ij}\tilde{T}'_{ij}\tilde{B}_i).
\end{aligned}$$

It is clear here that there are $2n$ columns dedicated to $\frac{\partial \tilde{p}_{ij}}{\partial \boldsymbol{m}_{hl}}$'s, 2 columns for $\frac{\partial \tilde{p}_{ij}}{\partial \tilde{x}_c}$ and $\frac{\partial \tilde{p}_{ij}}{\partial \tilde{y}_c}$, and $3 \times k$ columns for $\frac{\partial \tilde{p}_{ij}}{\partial \tilde{A}_i}$, $\frac{\partial \tilde{p}_{ij}}{\partial \tilde{B}_i}$, and $\frac{\partial \tilde{p}_{ij}}{\partial \tilde{\psi}_i}$. Therefore, $\boldsymbol{F}$ can be written in the compact form $\boldsymbol{F}_{n\times m} = (\boldsymbol{C}_{n\times 2n} \quad \boldsymbol{S}_{n\times d})$, where

$$\boldsymbol{C} = \begin{pmatrix} \boldsymbol{C}_1 & & & \\ & \boldsymbol{C}_2 & & \\ & & \ddots & \\ & & & \boldsymbol{C}_k \end{pmatrix}_{n\times 2n}, \quad \boldsymbol{C}_i = \begin{pmatrix} \tilde{\boldsymbol{r}}_{i1}^{\top} & & & \\ & \tilde{\boldsymbol{r}}_{i2}^{\top} & & \\ & & \ddots & \\ & & & \tilde{\boldsymbol{r}}_{in_i}^{\top} \end{pmatrix}_{n_i\times 2n_i}, \tag{9}$$

and

$$\tilde{\boldsymbol{r}}_{ij} = \nabla_{(\tilde{x},\tilde{y})}\tilde{p}_{ij} = 2\left(\tilde{T}_{ij}\tilde{A}_i\tilde{C}_i - \tilde{T}'_{ij}\tilde{B}_i\tilde{S}_i, \tilde{T}_{ij}\tilde{A}_i\tilde{S}_i + \tilde{T}'_{ij}\tilde{B}_i\tilde{C}_i\right)^{\top}. \tag{10}$$

Here $\boldsymbol{C}_i$ is an $n_i \times 2n_i$ matrix that has j^{th} row equal to $(\frac{\partial \tilde{p}_{ij}}{\partial \tilde{\boldsymbol{m}}_{11}^{\top}}, \ldots, \frac{\partial \tilde{p}_{ij}}{\partial \tilde{\boldsymbol{m}}_{1n_1}^{\top}}, \ldots, \frac{\partial \tilde{p}_{ij}}{\partial \tilde{\boldsymbol{m}}_{k1}^{\top}}, \ldots, \frac{\partial \tilde{p}_{ij}}{\partial \tilde{\boldsymbol{m}}_{kn_k}^{\top}})_{1\times 2n_i}$. The $n \times d$ matrix $\boldsymbol{S}$ is defined as

$$\boldsymbol{S} = \begin{pmatrix} \boldsymbol{R}_1 & \boldsymbol{S}_1 & & \\ \boldsymbol{R}_2 & & \boldsymbol{S}_2 & \\ \vdots & & & \ddots \\ \boldsymbol{R}_k & & & \boldsymbol{S}_k \end{pmatrix}_{n\times d}, \tag{11}$$

where the j^{th} of $\boldsymbol{R}_i$ and $\boldsymbol{S}_i$ are, respectively, equal to

$$\nabla_{(\tilde{x}_c,\tilde{y}_c)}\tilde{p}_{ij} = -2\left(\tilde{T}_{ij}\tilde{A}_i\tilde{C}_i - \tilde{T}'_{ij}\tilde{B}_i\tilde{S}_i, \tilde{T}_{ij}\tilde{A}_i\tilde{S}_i + \tilde{T}'_{ij}\tilde{B}_i\tilde{C}_i\right) \tag{12}$$

and $\nabla_{(\tilde{A}_i,\tilde{B}_i,\tilde{\psi}_i)}\tilde{p}_{ij} = \left(\tilde{T}_{ij}^2, \tilde{T}_{ij}'^2, 2\tilde{T}_{ij}\tilde{T}_{ij}'(\tilde{A}_i - \tilde{B}_i)\right)$. For this structure of $\boldsymbol{F}$, we need to find $\boldsymbol{U}$ such that $\boldsymbol{FU} = \boldsymbol{0}_{n\times(m-n)}$. If we define

$$\boldsymbol{U} = \begin{pmatrix} \boldsymbol{C}^{\perp}_{2n\times n} & \boldsymbol{V}_{2n\times d} \\ \boldsymbol{0}_{(2+3k)\times n} & \boldsymbol{I}_d \end{pmatrix}_{m\times m-n}, \quad \boldsymbol{C}_i^{\perp} = \begin{pmatrix} (\tilde{\boldsymbol{r}}_{i1}^{\perp})^{\top} & & & \\ & (\tilde{\boldsymbol{r}}_{i2}^{\perp})^{\top} & & \\ & & \ddots & \\ & & & (\tilde{\boldsymbol{r}}_{in_i}^{\perp})^{\top} \end{pmatrix}_{2n_i\times n_i}$$

with $\tilde{\boldsymbol{r}}_{ij}^{\perp} = 2\left(\tilde{T}_{ij}\tilde{A}_i\tilde{S}_i + \tilde{T}_{ij}'\tilde{B}_i\tilde{C}_i, \tilde{T}_{ij}'\tilde{B}_i\tilde{S}_i - \tilde{T}_{ij}\tilde{A}_i\tilde{C}_i\right)^{\top}$. Now it is easy to see that $\boldsymbol{CC}^{\perp} = \boldsymbol{0}_{n\times n}$. Thus, in order to show that $\boldsymbol{FU} = \boldsymbol{0}_{n\times(m-n)}$ we need to define $\boldsymbol{V}$ such that $\boldsymbol{CV} + \boldsymbol{S} = \boldsymbol{0}_{n\times d}$. If we define

$$\boldsymbol{V} = \begin{pmatrix} \boldsymbol{I}_2 & \boldsymbol{V}_1 & & \\ \vdots & & \boldsymbol{V}_2 & \\ \vdots & & & \ddots \\ \boldsymbol{I}_2 & & & \boldsymbol{V}_k \end{pmatrix}_{2n\times d}, \quad \boldsymbol{V}_i = \begin{pmatrix} -\tilde{T}_{i1}^2\tilde{\boldsymbol{u}}_{i1} & -\tilde{T}_{i1}'^2\tilde{\boldsymbol{u}}_{i1} & -2\tilde{T}_{i1}\tilde{T}_{i1}'(\tilde{A}_i - \tilde{B}_i)\tilde{\boldsymbol{u}}_{i1} \\ \vdots & \vdots & \vdots \\ -\tilde{T}_{in_i}^2\tilde{\boldsymbol{u}}_{in_i} & -\tilde{T}_{in_i}'^2\tilde{\boldsymbol{u}}_{in_i} & -2\tilde{T}_{in_i}\tilde{T}_{in_i}'(\tilde{A}_i - \tilde{B}_i)\tilde{\boldsymbol{u}}_{in_i} \end{pmatrix}_{2n_i\times 3},$$

where $\tilde{\boldsymbol{u}}_{ij} = \frac{\tilde{\boldsymbol{r}}_{ij}}{\|\tilde{\boldsymbol{r}}_{ij}\|^2}$, then $\boldsymbol{CV} = -\boldsymbol{S}$. Thus, this choice of $\boldsymbol{U}$ satisfies $\boldsymbol{FU} = \boldsymbol{0}_{n\times(m-n)}$. Now, using the definition of $\boldsymbol{J}$, we have

$$\boldsymbol{U}^{\top}\boldsymbol{JU} = \begin{pmatrix} (\boldsymbol{C}^{\perp})^{\top}\boldsymbol{\Sigma}_{2n}^{-1}\boldsymbol{C}^{\perp} & (\boldsymbol{C}^{\perp})^{\top}\boldsymbol{\Sigma}_{2n}^{-1}\boldsymbol{V} \\ \boldsymbol{V}^{\top}\boldsymbol{\Sigma}_{2n}^{-1}\boldsymbol{C}^{\perp} & \boldsymbol{V}^{\top}\boldsymbol{\Sigma}_{2n}^{-1}\boldsymbol{V} \end{pmatrix}. \tag{13}$$

Next, we apply the following lemma in order to obtain the CCRB of $\hat{\boldsymbol{\phi}}$.

Lemma 1 If $\boldsymbol{A} = \begin{pmatrix} \boldsymbol{A_{11}}_{n\times n} & \boldsymbol{A_{12}}_{n\times p} \\ \boldsymbol{A_{21}}_{p\times n} & \boldsymbol{A_{22}}_{p\times p} \end{pmatrix}$ is an $(n+p)\times(n+p)$ matrix and $\boldsymbol{A_{22}}^{-1}$ exists, then the components of $\boldsymbol{B} = \boldsymbol{A}^{-1}$ is $\begin{pmatrix} \boldsymbol{B}_{11} & \boldsymbol{B}_{12} \\ \boldsymbol{B}_{21} & \boldsymbol{B}_{22} \end{pmatrix}$, where

$$\begin{aligned} \boldsymbol{B}_{11} &= \boldsymbol{A}_{11}^{-1} + \boldsymbol{A}_{11}^{-1}\boldsymbol{A}_{12}(\boldsymbol{A}_{22} - \boldsymbol{A}_{21}\boldsymbol{A}_{11}^{-1}\boldsymbol{A}_{12})^{-1}\boldsymbol{A}_{21}\boldsymbol{A}_{11}^{-1} \\ \boldsymbol{B}_{12} &= -\boldsymbol{A}_{11}^{-1}\boldsymbol{A}_{12}(\boldsymbol{A}_{22} - \boldsymbol{A}_{21}\boldsymbol{A}_{11}^{-1}\boldsymbol{A}_{12})^{-1} \\ \boldsymbol{B}_{22} &= (\boldsymbol{A}_{22} - \boldsymbol{A}_{21}\boldsymbol{A}_{11}^{-1}\boldsymbol{A}_{12})^{-1}. \end{aligned}$$

The CCRB of $\hat{\boldsymbol{\phi}}$. We are mainly interested in finding the lower bound for $\hat{\boldsymbol{\phi}}$. Because of the structure of $\boldsymbol{F}$, the bottom right block of $(\boldsymbol{U}^{\top}\boldsymbol{JU})^{-1}$ is all we are interested in. To obtain this, we apply Lemma 1 to (13). Accordingly,

the bottom right block matrix $(\boldsymbol{U}^\top \boldsymbol{J}\boldsymbol{U})^{-1}$ is

$$\begin{aligned}\boldsymbol{B}_{22} &= \left(\boldsymbol{V}^\top \boldsymbol{\Sigma}_{2n}^{-1}\boldsymbol{V} - \boldsymbol{V}^\top \boldsymbol{\Sigma}_{2n}^{-1}\boldsymbol{C}^\perp((\boldsymbol{C}^\perp)^\top \boldsymbol{\Sigma}_{2n}^{-1}\boldsymbol{C}^\perp)^{-1}(\boldsymbol{C}^\perp)^\top \boldsymbol{\Sigma}_{2n}^{-1}\boldsymbol{V}\right)^{-1} \\ &= \left(\boldsymbol{V}^\top \boldsymbol{\Sigma}_{2n}^{-1/2}\left(\boldsymbol{I}_d - \boldsymbol{D}(\boldsymbol{D}^\top \boldsymbol{D})^{-1}\boldsymbol{D}^\top\right)\boldsymbol{\Sigma}_{2n}^{-1/2}\boldsymbol{V}\right)^{-1},\end{aligned}$$

where $\boldsymbol{D} = \boldsymbol{\Sigma}_{2n}^{-1/2}\boldsymbol{C}^\perp$. It is worth mentioning here that $\boldsymbol{I}_d - \boldsymbol{D}(\boldsymbol{D}^\top \boldsymbol{D})^{-1}\boldsymbol{D}^\top$ is the projection matrix onto the orthogonal components of the column space of $\boldsymbol{D}$. Since $\boldsymbol{C}\boldsymbol{C}^\perp = \boldsymbol{0}$, then $\boldsymbol{D}^\perp = \boldsymbol{C}\boldsymbol{\Sigma}_{2n}^{1/2}$ and $\boldsymbol{D}$ are orthogonal. Then $\boldsymbol{I}_d - \boldsymbol{D}(\boldsymbol{D}^\top \boldsymbol{D})^{-1}\boldsymbol{D}^\top$ is the projection matrix onto the column space of $(\boldsymbol{D}^\perp)^\top$. This implies that $\boldsymbol{I}_d - \boldsymbol{D}(\boldsymbol{D}^\top \boldsymbol{D})^{-1}\boldsymbol{D}^\top = (\boldsymbol{D}^\perp)^\top\left((\boldsymbol{D}^\perp)(\boldsymbol{D}^{\perp})^\top\right)^{-1}\boldsymbol{D}^\perp$. Accordingly, substituting $\boldsymbol{D}^\perp = \boldsymbol{C}\boldsymbol{\Sigma}_{2n}^{1/2}$ and using the fact $\boldsymbol{C}\boldsymbol{V} = -\boldsymbol{S}$ in $\boldsymbol{B}_{22}$ yield

$$\begin{aligned}\boldsymbol{B}_{22} &= \left(\boldsymbol{V}^\top \boldsymbol{\Sigma}_{2n}^{-1/2}(\boldsymbol{D}^\perp)^\top\left((\boldsymbol{D}^\perp)(\boldsymbol{D}^{\perp})^\top\right)^{-1}\boldsymbol{D}^\perp \boldsymbol{\Sigma}_{2n}^{-1/2}\boldsymbol{V}\right)^{-1} \\ &= \left(\boldsymbol{S}\left(\boldsymbol{D}^\perp(\boldsymbol{D}^\perp)^\top\right)^{-1}\boldsymbol{S}\right)^{-1} \\ &= \left(\boldsymbol{S}^\top\left(\boldsymbol{C}\boldsymbol{\Sigma}_{2n}\boldsymbol{C}^\top\right)^{-1}\boldsymbol{S}^\top\right)^{-1},\end{aligned} \tag{14}$$

and as such,

$$\mathrm{CCRB}(\hat{\boldsymbol{\phi}}) = \nabla_{\tilde{\boldsymbol{\phi}}}\mathbb{E}(\hat{\boldsymbol{\phi}})\left(\boldsymbol{S}^\top\left(\boldsymbol{C}\boldsymbol{\Sigma}_{2\mathrm{n}}\boldsymbol{C}^\top\right)^{-1}\boldsymbol{S}\right)^{-1}\nabla_{\tilde{\boldsymbol{\phi}}}\mathbb{E}(\hat{\boldsymbol{\phi}})^\top. \tag{15}$$

For the special case where $\boldsymbol{\Sigma}_{2n} = \sigma^2\boldsymbol{I}_{2n}$ is the covariance matrix of $\boldsymbol{n}$, (15) becomes $\mathrm{CCRB}(\hat{\boldsymbol{\phi}}) = \sigma^2\nabla_{\tilde{\boldsymbol{\phi}}}\mathbb{E}(\hat{\boldsymbol{\phi}})\left(\boldsymbol{S}^\top\left(\boldsymbol{C}\boldsymbol{C}^\top\right)^{-1}\boldsymbol{S}\right)^{-1}\nabla_{\tilde{\boldsymbol{\phi}}}\mathbb{E}(\hat{\boldsymbol{\phi}})^\top$.

The CCRB of $\tilde{\boldsymbol{m}}$. Although the estimation of the parameter vector $\tilde{\boldsymbol{\phi}}$ is our interest here, this general formula of the CCRB allows us to find the CCRB of the true points. In many engineering problems, it is important to estimate

the true points and establish their statistical properties, chief among them the CCRB. Although the following does not have any role in the sequel chapters, we would like to derive the CCRB of the true points. The analysis is similar to our derivation of the CCRB of $\hat{\boldsymbol{\phi}}$. Here we need to compute $\boldsymbol{B}_{11}$; i.e.,

$$\boldsymbol{B}_{11} = \left((\boldsymbol{C}^{\perp})^{\top}\boldsymbol{\Sigma}_{2n}^{-1}\boldsymbol{C}^{\perp}\right)^{-1}(\boldsymbol{C}^{\perp})^{\top}\boldsymbol{\Sigma}_{2n}^{-1/2}\left(\boldsymbol{I} + \boldsymbol{\Sigma}_{2n}^{-1/2}\boldsymbol{V}\boldsymbol{B}_{22}\boldsymbol{V}^{\top}\boldsymbol{\Sigma}_{2n}^{-1/2}\right)$$
$$\boldsymbol{\Sigma}_{2n}^{-1/2}\boldsymbol{C}^{\perp}\left((\boldsymbol{C}^{\perp})^{\top}\boldsymbol{\Sigma}_{2n}^{-1}\boldsymbol{C}^{\perp}\right)^{-1}.$$

4 Statistical Analysis

To assess the accuracy and precision of the two developed estimators, we will compare their variances to the CCRB. An estimator with variance equal to the CCRB is preferred over an estimator with variance greater than (15). In order to accomplish this task, we derive the leading terms of their *Total Mean Squared Error* TMSE($\hat{\boldsymbol{\phi}}$), which depends on the number of concentric ellipses. Without loss of generality, we will assume from now on that the number of concentric ellipses is $k = 2$. The extension of our algorithms to $k > 2$ case in this and next sections is rather simple, and hence, it is omitted here. Therefore, here we consider $\hat{\boldsymbol{\phi}} = \left(\hat{x}_c, \hat{y}_c, \hat{A}_1, \hat{B}_1, \hat{\psi}_1, \hat{A}_2, \hat{B}_2, \hat{\psi}_2\right)^{\top}$. Before proceeding, we will first introduce the so-called *small-sigma asymptotic regime* and *geometrically consistent estimator*.

Large Sample versus Small-sigma Regimes. It is common in statistics to study the asymptotic properties of estimators as $n \to \infty$. An estimator $\hat{\boldsymbol{\phi}}$ of $\tilde{\boldsymbol{\phi}}$ is said to be statistically *consistent* if $\hat{\boldsymbol{\phi}} \to \tilde{\boldsymbol{\phi}}$ as $n \to \infty$. In the context of the functional model, the true points are unobservable, and as such, they are regarded as nuisance parameters. Thus we have $2n + d$ parameters, where

n is the total number of observed points, and d is the number of parameters that characterizes the fitted geometric shape. The concern with functional models is that the number of parameters grows with n. For this reason, statisticians proposed the so-called a *small-sigma* models. Back in the early 1980s, Kunitomo (1980) developed an analytic approach to the studies of the estimators $\hat{a}$ and $\hat{b}$ of $y = a + bx$. They adopted a small-noise model, in which the number of observed points n is fixed (and not large) and the noise level σ is small and approaches zero. They used the Taylor expansion for the distribution functions of the estimators $\hat{a}$ and $\hat{b}$. Later Amemiya and Fuller (1988) adopted a 'hybrid' model in which $n \to \infty$ and $\sigma \to 0$ simultaneously so that $n\sigma^{\delta}$ remained constant for some $\delta > 0$. They also used the Taylor expansion in their analytic studies of the corresponding MLE. More recently Kanatani (2008) argued that the small-noise model is the most appropriate for computer vision and signal processing applications. He maintains that the whole set of observed points $\{\boldsymbol{m}_1, \ldots, \boldsymbol{m}_n\}$ (say) should be treated as *one single (multi-dimensional) observation*, rather than a sample of size n from a population. Therefore, the asymptotic quality of estimators will be analyzed here in the limit $\sigma \to 0$ instead of $n \to \infty$.

Geometrically Consistent Estimator. With a small-sigma model, an estimator $\hat{\boldsymbol{\phi}}$ is said to be a *geometrically consistent* estimator of $\tilde{\boldsymbol{\phi}}$ if $\hat{\boldsymbol{\phi}} \to \tilde{\boldsymbol{\phi}}$ as $\sigma \to 0$. This model is more appropriate for dealing with digitized pixel data since the number of observations is usually limited, whereas the deviance of an observation from its true point is desired to be small. Now we turn our attention to studying the statistical properties of each estimator. Since there are no explicit expressions of both estimators, we will use the Taylor expansion to get their linear approximations. Using the fact that both estimators are geometrically consistent of $\tilde{\boldsymbol{\phi}}$ and expanding both estimators about their true values,

we obtain their linear approximations; i.e., $\hat{\boldsymbol{\phi}}_{\mathrm{L}} = \tilde{\boldsymbol{\phi}} + \Delta_1\hat{\boldsymbol{\phi}}_{\mathrm{L}} + \mathcal{O}_{\mathrm{P}}(\sigma^2)$ and $\hat{\boldsymbol{\phi}}_{\mathrm{G}} = \tilde{\boldsymbol{\phi}} + \Delta_1\hat{\boldsymbol{\phi}}_{\mathrm{G}} + \mathcal{O}_{\mathrm{P}}(\sigma^2)$. Thus, up the first order, the TMSE of $\hat{\boldsymbol{\phi}}$ equals to $\mathrm{Var}(\Delta_1\hat{\boldsymbol{\phi}})$. Accordingly, we will focus now on deriving $\Delta_1\hat{\boldsymbol{\phi}}$ for each estimator and the corresponding variances.

To find $\Delta_1\hat{\boldsymbol{\phi}}$'s, we emphasize here that $\hat{\boldsymbol{\phi}}_{\mathrm{L}}$ and $\hat{\boldsymbol{\phi}}_{\mathrm{G}}$ minimize $\mathcal{F}_{\mathrm{L}}(\boldsymbol{\phi})$ and $\mathcal{F}_{\mathrm{G}}(\boldsymbol{\phi})$, respectively. To extract the leading term $\Delta_1\hat{\boldsymbol{\phi}}$ of each estimator from $\mathcal{F}_{\mathrm{L}}(\hat{\boldsymbol{\phi}}_{\mathrm{L}})$ and $\mathcal{F}_{\mathrm{G}}(\hat{\boldsymbol{\phi}}_{\mathrm{G}})$, we set $\nabla_{\Delta_1\hat{\boldsymbol{\phi}}}\mathcal{F}(\hat{\boldsymbol{\phi}}) = \mathbf{0}$ and express $\Delta_1\hat{\boldsymbol{\phi}}$ in terms of $\boldsymbol{n}$. Since both estimators use p_{ij} in the objective function, we need to express $\hat{p}_{ij} = \hat{p}_{ij}(\hat{\boldsymbol{\phi}})$ in terms of $\Delta_1\hat{\boldsymbol{\phi}}$. To accomplish this we expand $\hat{p}_{ij}$ about its true value $\tilde{p}_{ij} = 0$, which is true due to the fact that the true point lies on the true curve; i.e., $\tilde{p}_{ij} = \tilde{T}_{ij}^2\tilde{A}_i + \tilde{T}_{ij}'^2\tilde{B}_i - 1 = 0$. Therefore, after simple algebra one can show that $\hat{p}_{ij} = \Delta_1\hat{p}_{ij} + \mathcal{O}_{\mathrm{P}}(\sigma^2)$, where

$$\Delta_1\hat{p}_{ij} = 2\tilde{T}_{ij}\tilde{A}_i\Delta_1T_{ij} + 2\tilde{T}_{ij}'\tilde{B}_i\Delta_1T_{ij}' + \tilde{T}_{ij}^2\Delta_1\hat{A}_i + \tilde{T}_{ij}'^2\Delta_1\hat{B}_i. \tag{16}$$

But T_{ij} and T_{ij}' are also functions of $\hat{\boldsymbol{\phi}}$. Using the fact that

$$\cos(\hat{\psi}_i) = \tilde{C}_i - \tilde{S}_i\Delta_1\hat{\psi}_i + \mathcal{O}_{\mathrm{P}}(\sigma^2) \qquad \text{and} \qquad \sin(\hat{\psi}_i) = \tilde{S}_i + \tilde{C}_i\Delta_1\hat{\psi}_i + \mathcal{O}_{\mathrm{P}}(\sigma^2),$$

where $\tilde{C}_i = \cos(\tilde{\psi}_i)$ and $\tilde{S}_i = \sin(\tilde{\psi}_i)$ for $i = 1, 2$, one can show that

$$\Delta_1T_{ij} = \boldsymbol{\tau}_{ij}^{\top}\Delta_1\hat{\boldsymbol{\phi}} + \boldsymbol{l}_i^{\top}\boldsymbol{n}_{ij} \qquad \Delta_1T_{ij}' = \boldsymbol{\tau}_{ij}'^{\top}\Delta_1\hat{\boldsymbol{\phi}} + \boldsymbol{l}_i^{\perp\top}\boldsymbol{n}_{ij}, \tag{17}$$

where

$$\begin{aligned}
\boldsymbol{l}_i &= \left(\tilde{C}_i, \tilde{S}_i\right)^\top \\
\boldsymbol{l}_i^\perp &= \left(-\tilde{S}_i, \tilde{C}_i\right)^\top \\
\boldsymbol{\tau}_{ij} &= \left(-\boldsymbol{l}^\top, 0, 0, \tilde{T}'_{1j}\hat{\delta}_{1i}, 0, 0, \tilde{T}'_{2j}\hat{\delta}_{2i}\right)^\top \\
\boldsymbol{\tau}'_{ij} &= \left(-(\boldsymbol{l}^\perp)^\top, 0, 0, -\tilde{T}_{1j}\hat{\delta}_{1i}, 0, 0, -\tilde{T}_{2j}\hat{\delta}_{2i}\right)^\top,
\end{aligned} \tag{18}$$

where $\hat{\delta}_{ki}$ stands for the Dirac delta function; i.e., $\hat{\delta}_{ki} = 1$ when $i = k$ and zero otherwise. Putting these equations together we will be able to express $\Delta_1\hat{p}_{ij}$ as follows:

Lemma 2 Let $\hat{\boldsymbol{\phi}} = \arg\min \mathcal{F}(\hat{\boldsymbol{\phi}})$, where $\mathcal{F}$ is either $\mathcal{F}_{\mathrm{L}}$ or $\mathcal{F}_{\mathrm{G}}$ and define $\hat{p}_{ij} = T_{ij}^2\hat{A}_i + T_{ij}^{'2}\hat{B}_i - 1$, where $T_{ij} = \big(x_{ij} - \hat{x}_c\big)\cos(\hat{\psi}_i) + \big(y_{ij} - \hat{y}_c\big)\sin(\hat{\psi}_i)$ and $T'_{ij} = -\big(x_{ij} - \hat{x}_c\big)\sin(\hat{\psi}_i) + \big(y_{ij} - \hat{y}_c\big)\cos(\hat{\psi}_i)$. Then

$$\Delta_1\hat{p}_{ij} = 2\tilde{\boldsymbol{q}}_{ij}^\top\Delta_1\hat{\boldsymbol{\phi}} + 2\tilde{\boldsymbol{z}}_{ij}^\top\boldsymbol{n}_{ij}, \tag{19}$$

where

$$\tilde{\boldsymbol{z}}_{ij}^\top = \left(\tilde{T}_{ij}\tilde{A}_i\tilde{C}_i - \tilde{T}'_{ij}\tilde{B}_i\tilde{S}_i, \tilde{T}_{ij}\tilde{A}_i\tilde{S}_i + \tilde{T}'_{ij}\tilde{B}_i\tilde{C}_i\right), \tag{20}$$

$$\tilde{\boldsymbol{q}}_{ij}^\top = \left(-\tilde{\boldsymbol{z}}_{ij}^\top, \frac{\hat{\delta}_{1i}\tilde{T}_{1j}^2}{2}, \frac{\hat{\delta}_{1i}\tilde{T}_{1j}^{'2}}{2}, \hat{\delta}_{1i}\tilde{T}_{1j}\tilde{T}'_{1j}(\tilde{A}_1 - \tilde{B}_1), \frac{\hat{\delta}_{2i}\tilde{T}_{2j}^2}{2}, \frac{\hat{\delta}_{2i}\tilde{T}_{2j}^{'2}}{2}, \hat{\delta}_{2i}\tilde{T}_{2j}\tilde{T}'_{2j}(\tilde{A}_2 - \tilde{B}_2)\right).$$

The useful facts summarized in Lemma 2 will be commonly used in the analysis of both the LS and the GRAF estimators, and as such, help us derive $\Delta_1\hat{\boldsymbol{\phi}}_{\mathrm{L}}$ and $\Delta_1\hat{\boldsymbol{\phi}}_{\mathrm{G}}$ and their variances.

First-Order Error Analysis of LS. Since $\hat{\boldsymbol{\phi}}_{\mathrm{L}}$ is the minimizer of $\mathcal{F}_{\mathrm{L}}$. Then up to order σ^2, we have

$$\mathcal{F}_{\mathrm{L}}(\hat{\boldsymbol{\phi}}_{\mathrm{L}}) = \sum_{i=1}^{2}\sum_{j=1}^{n_i}(\hat{p}_{ij})^2 = \sum_{i=1}^{2}\sum_{j=1}^{n_i}(\tilde{p}_{ij} + \Delta_1\hat{p}_{ij})^2 = \sum_{i=1}^{2}\sum_{j=1}^{n_i}(\Delta_1\hat{p}_{ij})^2, \tag{21}$$

where $\Delta_1\hat{p}_{ij}$ is given in (19). Let us now denote $\hat{\boldsymbol{p}} = (\hat{p}_{11}, \ldots, \hat{p}_{1n_1}, \ldots \hat{p}_{2n_2})^\top$, and let $\tilde{\boldsymbol{Z}}_{n\times 2n}$ be the matrix $\tilde{\boldsymbol{Z}} = \mathrm{Diag}(\tilde{\boldsymbol{z}}_{11}^\top, \ldots, \tilde{\boldsymbol{z}}_{1n_1}^\top, \tilde{\boldsymbol{z}}_{21}^\top, \ldots, \tilde{\boldsymbol{z}}_{2n_2}^\top)$, where $\tilde{\boldsymbol{z}}_{ij}$'s are given in (20). Then $\mathcal{F}_{\mathrm{L}}(\hat{\boldsymbol{\phi}}_{\mathrm{L}})$ can be expressed as

$$\mathcal{F}_{\mathrm{L}}(\hat{\boldsymbol{\phi}}_{\mathrm{L}}) = \|\hat{\boldsymbol{p}}\|^2 = 4\|\tilde{\boldsymbol{Q}}\Delta_1\hat{\boldsymbol{\phi}}_{\mathrm{L}} + \tilde{\boldsymbol{Z}}\boldsymbol{n}\|^2 + \mathcal{O}_{\mathrm{P}}(\sigma^2), \tag{22}$$

where

$$\tilde{\boldsymbol{Q}} = \begin{pmatrix} \tilde{\boldsymbol{Q}}_{11} & \tilde{\boldsymbol{Q}}_{12} & \mathbf{0}_{n_1\times 3} \\ \tilde{\boldsymbol{Q}}_{21} & \mathbf{0}_{n_2\times 3} & \tilde{\boldsymbol{Q}}_{22} \end{pmatrix}_{n\times 8}. \tag{23}$$

The exact expressions of the block matrices $\tilde{\tilde{\boldsymbol{Q}}}_{i1}$ and $\tilde{\tilde{\boldsymbol{Q}}}_{i2}$ are

$$\tilde{\boldsymbol{Q}}_{i1} = \begin{pmatrix} -\tilde{\boldsymbol{z}}_{i1}^\top \\ \vdots \\ -\tilde{\boldsymbol{z}}_{in_i}^\top \end{pmatrix}_{n_i\times 2}, \tilde{\boldsymbol{Q}}_{i2} = \begin{pmatrix} \frac{1}{2}\tilde{T}_{i1}^2 & \frac{1}{2}\tilde{T}_{i1}'^2 & \tilde{T}_{i1}\tilde{T}_{i1}'(\tilde{A}_i - \tilde{B}_i) \\ \vdots & \vdots & \vdots \\ \frac{1}{2}\tilde{T}_{in_i}^2 & \frac{1}{2}\tilde{T}_{in_i}'^2 & \tilde{T}_{in_i}\tilde{T}_{in_i}'(\tilde{A}_i - \tilde{B}_i) \end{pmatrix}_{n_i\times 3}. \tag{24}$$

We would like to minimize the objective function (22). We differentiate the right-hand side of (22) with respect to $\Delta_1\hat{\boldsymbol{\phi}}_{\mathrm{L}}$ and set it equal to zero to obtain

$$\Delta_1\hat{\boldsymbol{\phi}}_{\mathrm{L}} = -(\tilde{\boldsymbol{Q}}^\top\tilde{\boldsymbol{Q}})^{-1}\tilde{\boldsymbol{Q}}^\top\tilde{\boldsymbol{Z}}\boldsymbol{n}. \tag{25}$$

It is clear that $\Delta_1\hat{\boldsymbol{\phi}}_{\mathrm{L}}$ is a linear form of $\boldsymbol{n}$, and as such, it will have zero expectations. Let us now compute the variance of $\Delta_1\hat{\boldsymbol{\phi}}_{\mathrm{L}}$.

$$\mathrm{Var}(\Delta_1\hat{\boldsymbol{\phi}}_{\mathrm{L}}) = (\tilde{\boldsymbol{Q}}^\top\tilde{\boldsymbol{Q}})^{-1}\tilde{\boldsymbol{Q}}^\top\tilde{\boldsymbol{Z}}\mathbb{E}\left(\boldsymbol{n}\boldsymbol{n}^\top\right)\tilde{\boldsymbol{Z}}^\top\tilde{\boldsymbol{Q}}(\tilde{\boldsymbol{Q}}^\top\tilde{\boldsymbol{Q}})^{-1}. \tag{26}$$

Based on our assumption that $\mathrm{E}(\boldsymbol{n}\boldsymbol{n}^\top) = \boldsymbol{\Sigma}_{2\mathrm{n}} = \sigma^2\boldsymbol{I}_{2\mathrm{n}}$, we obtain

$$\mathrm{Var}(\Delta_1\hat{\boldsymbol{\phi}}_{\mathrm{L}}) = \sigma^2(\tilde{\boldsymbol{Q}}^\top\tilde{\boldsymbol{Q}})^{-1}\tilde{\boldsymbol{Q}}^\top\tilde{\boldsymbol{Z}}\tilde{\boldsymbol{Z}}^\top\tilde{\boldsymbol{Q}}(\tilde{\boldsymbol{Q}}^\top\tilde{\boldsymbol{Q}})^{-1}. \tag{27}$$

First-Order Error Analysis of GRAF. To conduct the first-order error analysis of $\hat{\boldsymbol{\phi}}_{\mathrm{G}}$, which is defined by

$$\hat{\boldsymbol{\phi}}_{\mathrm{G}} = \arg\min_{\boldsymbol{\phi}} \mathcal{F}_{\mathrm{G}}(\boldsymbol{\phi}) = \sum_{i=1}^{2}\sum_{j=1}^{n_i} \frac{\hat{p}_{ij}^2}{\|\nabla \hat{p}_{ij}\|^2}. \tag{28}$$

We will conduct a similar analysis as that of the LS estimator. Let us first define

$$w_{ij} := \frac{1}{4}\|\nabla p_{ij}\|^2 = \left(T_{ij}^2 A_i^2 + T_{ij}^{'2} B_i^2\right). \tag{29}$$

Now we expand $\mathcal{F}_{\mathrm{G}}(\hat{\boldsymbol{\phi}}_{\mathrm{G}})$ by perturbing $\hat{p}_{ij}$ and $\hat{w}_{ij}$ around their true points to obtain

$$\begin{aligned}
\mathcal{F}_{\mathrm{G}}(\hat{\boldsymbol{\phi}}_{\mathrm{G}}) &= \sum_{i=1}^{2}\sum_{j=1}^{n_i} \frac{(\tilde{p}_{ij} + \Delta_1 \hat{p}_{ij})^2}{4\tilde{w}_{ij} + 4\Delta_1 \hat{w}_{ij}} + \mathcal{O}_{\mathrm{P}}(\sigma^3) \\
&= \sum_{i=1}^{2}\sum_{j=1}^{n_i} \frac{\Delta_1 \hat{p}_{ij}^2}{4\tilde{w}_{ij}\left(\frac{\Delta_1 \hat{w}_{ij}}{\tilde{w}_{ij}} + 1\right)} + \mathcal{O}_{\mathrm{P}}(\sigma^3) \\
&= \sum_{i=1}^{2}\sum_{j=1}^{n_i} \frac{\Delta_1 \hat{p}_{ij}^2}{4\tilde{w}_{ij}} + \mathcal{O}_{\mathrm{P}}(\sigma^3).
\end{aligned}$$

Here we used $\frac{1}{1+x} = 1 - x + x^2 + \cdots$ but because $(\Delta_1 \hat{p}_{ij})^2 \sim \mathcal{O}_{\mathrm{P}}(\sigma^2/\sqrt{n})$, we only used the first term of $(1+x)^{-1}$. In vector notations, $\mathcal{F}_{\mathrm{G}}(\hat{\boldsymbol{\phi}}_{\mathrm{G}})$ can be expressed as a quadratic form of $\Delta_1 \hat{\boldsymbol{\phi}}_{\mathrm{G}}$. i.e.,

$$\mathcal{F}_{\mathrm{G}}(\hat{\boldsymbol{\phi}}_{\mathrm{G}}) = \|\tilde{\boldsymbol{Q}}_w \Delta_1 \hat{\boldsymbol{\phi}}_{\mathrm{G}} + \tilde{\boldsymbol{Z}}_w \boldsymbol{n}\|^2 + \mathcal{O}(\sigma^2), \tag{30}$$

where $\tilde{\boldsymbol{Z}}_w = \text{Diag}\left(\frac{\tilde{\boldsymbol{z}}_{11}^\top}{\sqrt{\tilde{w}_{11}}}, \ldots, \frac{\tilde{\boldsymbol{z}}_{1n_1}^\top}{\sqrt{\tilde{w}_{1n_1}}}, \frac{\tilde{\boldsymbol{z}}_{21}^\top}{\sqrt{\tilde{w}_{21}}}, \ldots, \frac{\tilde{\boldsymbol{z}}_{2n_2}^\top}{\sqrt{\tilde{w}_{2n_2}}}\right)$, while

$$\tilde{\boldsymbol{Q}}_w = \begin{pmatrix} \tilde{\boldsymbol{Q}}_{w11} & \tilde{\boldsymbol{Q}}_{w12} & \boldsymbol{0}_{n_1\times 3} \\ \tilde{\boldsymbol{Q}}_{w21} & \boldsymbol{0}_{n_2\times 3} & \tilde{\boldsymbol{Q}}_{w22} \end{pmatrix}_{n\times 8}, \qquad \tilde{\boldsymbol{Q}}_{wi1} = \begin{pmatrix} -\tilde{w}_{i1}^{-1/2}\tilde{\boldsymbol{z}}_{i1}^\top \\ \vdots \\ -\tilde{w}_{in_i}^{-1/2}\tilde{\boldsymbol{z}}_{in_i}^\top \end{pmatrix}_{n_i\times 2}, \tag{31}$$

and

$$\tilde{\boldsymbol{Q}}_{wi2} = \begin{pmatrix} \tilde{w}_{i1}^{-1/2}(\frac{1}{2}\tilde{T}_{i1}^2) & \tilde{w}_{i1}^{-1/2}(\frac{1}{2}\tilde{T}_{i1}'^2) & \tilde{w}_{i1}^{-1/2}\tilde{T}_{i1}\tilde{T}_{i1}'(\tilde{A}_i - \tilde{B}_i) \\ \vdots & \vdots & \vdots \\ \tilde{w}_{in_i}^{-1/2}(\frac{1}{2}\tilde{T}_{in_i}^2) & \tilde{w}_{in_i}^{-1/2}(\frac{1}{2}\tilde{T}_{in_i}'^2) & \tilde{w}_{in_i}^{-1/2}\tilde{T}_{in_i}\tilde{T}_{in_i}'(\tilde{A}_i - \tilde{B}_i) \end{pmatrix}_{n_i\times 3}. \tag{32}$$

Differentiating $\mathcal{F}_{\text{G}}$ with respect to $\Delta_1\hat{\boldsymbol{\phi}}_{\text{G}}$ and setting it to zero gives us

$$\Delta_1\hat{\boldsymbol{\phi}}_{\text{G}} = -(\tilde{\boldsymbol{Q}}_w^\top\tilde{\boldsymbol{Q}}_w)^{-1}\tilde{\boldsymbol{Q}}_w^\top\tilde{\boldsymbol{Z}}_w\boldsymbol{n}. \tag{33}$$

In turn, computing the variance of $\Delta_1\hat{\boldsymbol{\phi}}_{\text{G}}$ yields

$$\text{Var}(\Delta_1\hat{\boldsymbol{\phi}}_{\text{G}}) = (\tilde{\boldsymbol{Q}}_w^\top\tilde{\boldsymbol{Q}}_w)^{-1}\tilde{\boldsymbol{Q}}_w^\top\tilde{\boldsymbol{Z}}_w\text{Var}(\boldsymbol{n})\tilde{\boldsymbol{Z}}_w^\top\tilde{\boldsymbol{Q}}_w(\tilde{\boldsymbol{Q}}_w^\top\tilde{\boldsymbol{Q}}_w)^{-1}. \tag{34}$$

By our assumptions, $\text{Var}(\boldsymbol{n}) = \sigma^2\boldsymbol{I}_{n\times n}$ and $\tilde{\boldsymbol{Z}}_w\tilde{\boldsymbol{Z}}_w^\top = \boldsymbol{I}_{n\times n}$, therefore, (34) can be reduced to

$$\text{Var}(\Delta_1\hat{\boldsymbol{\phi}}_{\text{G}}) = \sigma^2(\tilde{\boldsymbol{Q}}_w^\top\tilde{\boldsymbol{Q}}_w)^{-1}. \tag{35}$$

Comparison with CCRB. It is of our interest to compare the leading term variance of both estimators with the CCRB. To do this, we will first simplify the CCRB in terms of $\tilde{\boldsymbol{Q}}_w$ Since $\boldsymbol{\Sigma}_{2n} = \sigma^2\boldsymbol{I}_{2n}$ and $\boldsymbol{C}\boldsymbol{C}^\top = \text{Diag}\left(\|\tilde{\boldsymbol{r}}_{11}\|^2, \ldots, \|\tilde{\boldsymbol{r}}_{kn_k}\|^2\right)$, where $\|\tilde{\boldsymbol{r}}_{ij}\|^2 = (\tilde{T}_{ij}\tilde{A}_i)^2 + (\tilde{T}_{ij}'\tilde{B}_i)^2$, one has $(\boldsymbol{C}\boldsymbol{C}^\top)^{-1} = \text{Diag}\left(\frac{1}{\|\tilde{\boldsymbol{r}}_{11}\|^2}, \ldots, \frac{1}{\|\tilde{\boldsymbol{r}}_{kn_k}\|^2}\right)$. Now after some algebraic

manipulations we obtain $\boldsymbol{S}^\top(\boldsymbol{C}\boldsymbol{C}^\top)^{-1}\boldsymbol{S} = \tilde{\boldsymbol{Q}}_w^\top\tilde{\boldsymbol{Q}}_w$. Hence, (15) is reduced to

$$\mathrm{CCRB}(\hat{\boldsymbol{\phi}}) = \sigma^2\nabla_{\tilde{\boldsymbol{\phi}}}\mathbb{E}(\hat{\boldsymbol{\phi}})(\tilde{\boldsymbol{Q}}_w^\top\tilde{\boldsymbol{Q}}_w)^{-1}\nabla_{\tilde{\boldsymbol{\phi}}}\mathbb{E}(\hat{\boldsymbol{\phi}})^\top. \tag{36}$$

Thus up to the leading term $\mathrm{Var}(\hat{\boldsymbol{\phi}}) \geq \sigma^2(\tilde{\boldsymbol{Q}}_w^\top\tilde{\boldsymbol{Q}}_w)^{-1}$, which coincides with (35) only. This shines a light on the motivation behind GRAF. Indeed, (35) is equal to the CCRB (36) up to order σ^2. With this, it is an optimal estimator, in that it achieves the theoretical lower bound on the variance of an estimator obtained from our model, while the LS is not optimal.

5 Estimator of Noise Parameter $\boldsymbol{\sigma^2}$

It is of interest to estimate the noise level σ^2, which can immediately be estimated after the parameter is estimated. To derive the estimator of σ^2 we use the first-order analysis. The variance of $\hat{\boldsymbol{\phi}}_{\mathrm{L}}$ and $\hat{\boldsymbol{\phi}}_{\mathrm{G}}$ depend on σ^2 and $\tilde{\boldsymbol{m}}_{ij}$, which is unknown under the functional model. Hence, to fully understand the accuracy of our estimators, we must provide an estimator for σ^2. We will use $\boldsymbol{m}_{ij}$ as a plug-in estimator of $\tilde{\boldsymbol{m}}_{ij}$, and as such, $\tilde{\boldsymbol{Q}}$, $\tilde{\boldsymbol{Q}}_w$, $\tilde{\boldsymbol{Z}}$ and $\tilde{\boldsymbol{Z}}_w$ will all be estimated by using the observed points $\boldsymbol{m}_{ij}$'s. These estimators will be denoted as $\boldsymbol{Q}$, $\boldsymbol{Q}_w$, $\boldsymbol{Z}$ and $\boldsymbol{Z}_w$, respectively. Our estimator of $\hat{\sigma}^2$ is

$$\hat{\sigma}^2 = c\mathcal{F}(\hat{\boldsymbol{\phi}}), \tag{37}$$

where c will be selected such that $\mathbb{E}(\hat{\sigma}^2) = \sigma^2$. Thus, we proceed by taking the expectation of (37) for each method.

5.1 LS-based Unbiased Estimator of σ^2

We will first estimate $\hat{\sigma}^2$ when LS estimator is implemented. Since $\mathbb{E}(\hat{\sigma}^2_{\mathrm{L}}) = c_{\mathrm{L}}\mathbb{E}\left(\mathcal{F}_{\mathrm{L}}(\hat{\boldsymbol{\phi}}_{\mathrm{L}})\right)$ and $\mathcal{F}_{\mathrm{L}}(\hat{\boldsymbol{\phi}}_{\mathrm{L}} = 4\|\boldsymbol{Q}\Delta_1\hat{\boldsymbol{\phi}}_{\mathrm{L}} + \boldsymbol{Z}\boldsymbol{n}\|^2 + \mathcal{O}_{\mathrm{P}}(\sigma^4)$, we obtain

$$\begin{aligned}\mathbb{E}(\hat{\sigma}^2_{\mathrm{L}}) &= c_{\mathrm{L}}\mathbb{E}\left(4\|(\tilde{\boldsymbol{Q}} + \Delta_1\boldsymbol{Q})\Delta_1\hat{\boldsymbol{\phi}}_{\mathrm{L}} + (\tilde{\boldsymbol{Z}} + \Delta_1\boldsymbol{Z}\right)\boldsymbol{n}\|^2) \\ &= c_{\mathrm{L}}\mathbb{E}\left(4\|\tilde{\boldsymbol{Q}}\Delta_1\hat{\boldsymbol{\phi}}_{\mathrm{L}} + \tilde{\boldsymbol{Z}}\boldsymbol{n}\|^2\right) + \mathcal{O}(\sigma^4).\end{aligned}$$

Thus, expanding $\|\tilde{\boldsymbol{Q}}\Delta_1\hat{\boldsymbol{\phi}}_{\mathrm{L}} + \tilde{\boldsymbol{Z}}\boldsymbol{n}\|^2$ and using (25) result in

$$\begin{aligned}\mathbb{E}(\hat{\sigma}^2_{\mathrm{L}}) &= 4c_{\mathrm{L}}\mathbb{E}\left(\Delta_1\hat{\boldsymbol{\phi}}_{\mathrm{L}}^\top\tilde{\boldsymbol{Q}}^\top\tilde{\boldsymbol{Q}}\Delta_1\hat{\boldsymbol{\phi}}_{\mathrm{L}} + 2\boldsymbol{n}^\top\tilde{\boldsymbol{Z}}^\top\tilde{\boldsymbol{Q}}\Delta_1\hat{\boldsymbol{\phi}}_{\mathrm{L}} + \boldsymbol{n}^\top\tilde{\boldsymbol{Z}}^\top\tilde{\boldsymbol{Z}}\boldsymbol{n}\right) + \mathcal{O}(\sigma^4) \\ &= 4c_{\mathrm{L}}\mathbb{E}\left(\boldsymbol{n}^\top\tilde{\boldsymbol{Z}}^\top\tilde{\boldsymbol{Q}}(\tilde{\boldsymbol{Q}}^\top\tilde{\boldsymbol{Q}})^{-1}\tilde{\boldsymbol{Q}}^\top\tilde{\boldsymbol{Z}}\boldsymbol{n} - 2\boldsymbol{n}^\top\tilde{\boldsymbol{Z}}^\top\tilde{\boldsymbol{Q}}(\tilde{\boldsymbol{Q}}^\top\tilde{\boldsymbol{Q}})^{-1}\tilde{\boldsymbol{Q}}^\top\tilde{\boldsymbol{Z}}\boldsymbol{n} + \boldsymbol{n}^\top\tilde{\boldsymbol{Z}}^\top\tilde{\boldsymbol{Z}}\boldsymbol{n}\right) + \mathcal{O}(\sigma^4) \\ &= 4\sigma^2c_{\mathrm{L}}\left(\mathrm{tr}(\tilde{\boldsymbol{Z}}^\top\tilde{\boldsymbol{Z}}) - \mathrm{tr}(\tilde{\boldsymbol{Z}}^\top\tilde{\boldsymbol{Q}}(\tilde{\boldsymbol{Q}}^\top\tilde{\boldsymbol{Q}})^{-1}\tilde{\boldsymbol{Q}}^\top\tilde{\boldsymbol{Z}})\right) + \mathcal{O}(\sigma^4).\end{aligned}$$

Therefore, c_{L} is $c_{\mathrm{L}} = \frac{1}{4\left(\mathrm{tr}(\boldsymbol{Z}^\top\boldsymbol{Z}) - \mathrm{tr}\left(\boldsymbol{Z}^\top\boldsymbol{Q}(\boldsymbol{Q}^\top\boldsymbol{Q})^{-1}\boldsymbol{Q}^\top\boldsymbol{Z}\right)\right)}$, which results in our choice of $\hat{\sigma}^2_{\mathrm{L}}$ to be $\hat{\sigma}^2_{\mathrm{L}} = c_{\mathrm{L}}\mathcal{F}_{\mathrm{L}}(\hat{\boldsymbol{\phi}}_{\mathrm{L}})$. In particular,

$$\hat{\sigma}^2_{\mathrm{L}} = \frac{\mathcal{F}_{\mathrm{L}}(\hat{\boldsymbol{\phi}}_{\mathrm{L}})}{4\left(\mathrm{tr}(\boldsymbol{Z}^\top\boldsymbol{Z}) - \mathrm{tr}\left(\boldsymbol{Z}^\top\boldsymbol{Q}(\boldsymbol{Q}^\top\boldsymbol{Q})^{-1}\boldsymbol{Q}^\top\boldsymbol{Z}\right)\right)}. \tag{38}$$

5.2 GRAF-based Unbiased Estimator of σ^2

Next, if GRAF is used to estimate $\hat{\boldsymbol{\phi}}$, we can use the GRAF-based $\hat{\boldsymbol{\phi}}$ to estimate $\hat{\sigma}^2_{\mathrm{G}}$. As before, our estimator will depend on a constant c_G, which is obtained by finding $\mathbb{E}(\hat{\sigma}^2_{\mathrm{G}})$. This process is identical to our findings in the LS. Since $\mathbb{E}(\hat{\sigma}^2_G) = c_{\mathrm{G}}\mathbb{E}(\mathcal{F}_{\mathrm{G}}(\hat{\boldsymbol{\phi}}_{\mathrm{G}}))$ and $\mathcal{F}_{\mathrm{G}}(\hat{\boldsymbol{\phi}}_{\mathrm{G}}) = \|\tilde{\boldsymbol{Q}}_w\Delta_1\hat{\boldsymbol{\phi}}_{\mathrm{G}} + \tilde{\boldsymbol{Z}}_w\boldsymbol{n}\|^2 + \mathcal{O}_{\mathrm{P}}(\sigma^4)$, we obtain

$$\begin{aligned}\mathbb{E}(\hat{\sigma}^2_G) &= \sigma^2c_{\mathrm{G}}\left(\mathrm{tr}(\tilde{\boldsymbol{Z}}_w^\top\tilde{\boldsymbol{Z}}_w) - \mathrm{tr}(\tilde{\boldsymbol{Z}}_w^\top\tilde{\boldsymbol{Q}}_w(\tilde{\boldsymbol{Q}}_w^\top\tilde{\boldsymbol{Q}}_w)^{-1}\tilde{\boldsymbol{Q}}_w^\top\tilde{\boldsymbol{Z}}_w)\right) + \mathcal{O}(\sigma^4) \\ &= \sigma^2c_{\mathrm{G}}\left(n - \mathrm{tr}(\tilde{\boldsymbol{Z}}_w^\top\tilde{\boldsymbol{Q}}_w(\tilde{\boldsymbol{Q}}_w^\top\tilde{\boldsymbol{Q}}_w)^{-1}\tilde{\boldsymbol{Q}}_w^\top\tilde{\boldsymbol{Z}}_w)\right) + \mathcal{O}(\sigma^4),\end{aligned}$$

where we used (33) and the fact that $\mathrm{tr}(\tilde{\boldsymbol{Z}}_w^\top \tilde{\boldsymbol{Z}}_w) = n$. Thus, $c_{\mathrm{G}} = \frac{1}{n-\mathrm{tr}\left(\boldsymbol{Z}_w^\top \boldsymbol{Q}_w (\boldsymbol{Q}_w^\top \boldsymbol{Q}_w)^{-1} \boldsymbol{Q}_w^\top \boldsymbol{Z}_w\right)}$ and our estimate of σ^2 using GRAF will be

$$\hat{\sigma}^2_{\mathrm{G}} = \frac{\mathcal{F}_{\mathrm{G}}(\hat{\boldsymbol{\phi}}_{\mathrm{G}})}{n - \mathrm{tr}\left(\boldsymbol{Z}_w^\top \boldsymbol{Q}_w (\boldsymbol{Q}_w^\top \boldsymbol{Q}_w)^{-1} \boldsymbol{Q}_w^\top \boldsymbol{Z}_w\right)}. \tag{39}$$

6 Numerical Implementation and Experiments

Due to nonlinearity of those two objective functions, numerical optimization techniques, such as gradient-decent methods, shall be implemented here. Those gradient-type methods need to evaluate the objective function and its gradients. For the sake of completion, we present them here using $k = 2$ only.

$$\nabla_{\boldsymbol{\phi}} \mathcal{F}_{\mathrm{L}}(\boldsymbol{\phi}) = \begin{pmatrix} \frac{\partial \mathcal{F}_{\mathrm{L}}}{\partial x_c} \\ \frac{\partial \mathcal{F}_{\mathrm{L}}}{\partial y_c} \\ \frac{\partial \mathcal{F}_{\mathrm{L}}}{\partial A_1} \\ \frac{\partial \mathcal{F}_{\mathrm{L}}}{\partial B_1} \\ \frac{\partial \mathcal{F}_{\mathrm{L}}}{\partial \psi_1} \\ \frac{\partial \mathcal{F}_{\mathrm{L}}}{\partial A_2} \\ \frac{\partial \mathcal{F}_{\mathrm{L}}}{\partial B_2} \\ \frac{\partial \mathcal{F}_{\mathrm{L}}}{\partial \psi_2} \end{pmatrix} = 4 \sum_{i=1}^{2} \sum_{j=1}^{n_i} \begin{pmatrix} p_{ij} \left(-T_{ij} A_i C_i + T'_{ij} B_i S_i\right) \\ p_{ij} \left(-T_{ij} A_i S_i - T'_{ij} B_i C_i\right) \\ \frac{1}{2} p_{1j} T_{1j}^2 \hat{\delta}_{1i} \\ \frac{1}{2} p_{1j} T_{1j}^{\prime 2} \hat{\delta}_{1i} \\ p_{1j} (T_{1j} T'_{1j} A_1 - T_{1j} T'_{1j} B_1) \hat{\delta}_{1i} \\ \frac{1}{2} p_{2j} T_{2j}^2 \hat{\delta}_{2i} \\ \frac{1}{2} p_{2j} T_{2j}^{\prime 2} \hat{\delta}_{2i} \\ p_{2j} (T_{2j} T'_{2j} A_2 - T_{2j} T'_{2j} B_2) \hat{\delta}_{2i} \end{pmatrix}, \tag{40}$$

and

$$\nabla \mathcal{F}_{\mathrm{G}}(\boldsymbol{\phi}) = \sum_{i=1}^{2} \sum_{j=1}^{n_i} \frac{1}{2w_{ij}^2} \begin{pmatrix} p_{ij}^2 \left(T_{ij} A_i^2 C_i - T'_{ij} B_i^2 S_i\right) - 2 p_{ij} w_{ij} \left(T_{ij} A_i C_i - T'_{ij} B_i S_i\right) \\ p_{ij}^2 \left(T_{ij} A_i^2 S_i + T'_{ij} B_i^2 C_i\right) - 2 p_{ij} w_{ij} \left(T_{ij} A_i S_i + T'_{ij} B_i C_i\right) \\ \left(p_{1j} w_{1j} T_{1j}^2 - p_{1j}^2 T_{1j}^2 A_1\right) \hat{\delta}_{1i} \\ \left(p_{1j} w_{1j} T_{1j}^{\prime 2} - p_{1j}^2 T_{1j}^{\prime 2} B_1\right) \hat{\delta}_{1i} \\ \left(2 p_{1j} w_{1j} T_{1j} T'_{1j} (A_1 - B_1) - p_{1j}^2 T_{1j} T'_{1j} (A_1^2 - B_1^2)\right) \hat{\delta}_{1i} \\ \left(p_{2j} w_{2j} T_{2j}^2 - p_{2j}^2 T_{2j}^2 A_2\right) \hat{\delta}_{2i} \\ \left(p_{2j} w_{2j} T_{2j}^{\prime 2} - p_{2j}^2 T_{2j}^{\prime 2} B_2\right) \hat{\delta}_{2i} \\ \left(2 p_{2j} w_{2j} T_{2j} T'_{2j} (A_2 - B_2) - p_{2j}^2 T_{2j} T_{2j} (A_2^2 - B_2^2)\right) \hat{\delta}_{2i}. \end{pmatrix}. \tag{41}$$

The Newton-Raphson method is a popular minimization method that converges fast when it converges. However, this method is very sensitive for the seeded initial guess. Therefore, we have implemented here other more robust iterative approaches, i.e., BFGS, L-BFGS-B, and Neder-Mead. It is well known that BFGS is one of the Quasi-Newton methods, where the approximation of

the Hessian matrix is updated with each iteration. The L-BFGS-B (or Limited memory-BFGS-Box) solves problems when some box constraints are imposed on the parametric space. The Nelder-Mead, on the other hand, s a much more complex algorithm than the previous two as it involves three steps per iteration (i.e., ordering, centroid, and transformation).

Moreover, all numerical algorithms depend on the initial guess that is seeded. This is a critical issue in order to improve convergence rate and convergence speed. Unfortunately, there is no explicit form for the initial guess. To tackle this issue, two initial guesses have been used to initialize those algorithms. Both approaches are the same in the first step but they differ in the second step. The first step in finding any initial guess requires firstly fitting of single ellipses via Taubin's method. The estimates of all parameters will be used except the center. To find an initial guess for the center we use the following two approaches. One approach is to take the average of the center estimates obtained in the first step. That is, if we denote by $\hat{\boldsymbol{\phi}}_i = (\hat{x}_{ci}, \hat{y}_{ci}, \hat{A}_i, \hat{B}_i, \hat{\psi}_i)^\top$, $i = 1, 2$, the estimates of parameters for each ellipse, then the initial guess will be $\hat{\boldsymbol{\phi}}_0 = (\frac{\hat{x}_{c1}+\hat{x}_{c2}}{2}, \frac{\hat{y}_{c1}+\hat{y}_{c2}}{2}, \hat{A}_1, \hat{B}_1, \hat{\psi}_1, \hat{A}_2, \hat{B}_2, \hat{\psi}_2)^\top$. The second approach is considering the pool of the data $\bar{x} = \frac{1}{n}\sum_{i=1}^{2}\sum_{j=1}^{n_i} x_{ij}$ and $\bar{y} = \frac{1}{n}\sum_{i=1}^{2}\sum_{j=1}^{n_i} y_{ij}$ where $n = n_1 + n_2$ as the initial guess for the center. Our numerical experiments show that the first approach is much better as it provides a better estimate of the estimate and leads to a better convergence rate.

6.1 Numerical Experiments

This section is devoted to numerical experiments and validation of our theory as described below. In our first set of experiments, we experimented with the three numerical schemes with the LS estimator only. The results obtained

for GRAF is similar and hence it is not shown here. In all our experiments, algorithms were seeded with the averaging initial guess.

In the first set of experiments, we ran several Monte-Carlo experiments, which help us shed more light on each of the three numerical schemes. There are several important factors in determining the best approach; namely, the divergence rate and the run-time till convergence. Of course, there are trade-offs to consider between the divergence rate and the average run time (ART). In our experiments, we used $n_1 = 20$ and $n_2 = 35$ equidistant points positioned on varying ellipse arc lengths with central angle $\rho = 120°, 180°$, and $240°$. The parameters of the two concentric ellipses were set to $a_1 = 2$, $b_1 = 1$, $\psi_1 = 0$, $a_2 = 3$, $b_2 = 2$, $\psi_2 = \frac{\pi}{4}$. We repeated the experiments $N = 2000$ times and used three methods: Nelder-Mead (dotted curve), BFGS (solid), L-BFGS-B (dashed) algorithms as shown in Figure 1. Figure 1 (top) shows the divergence rate of the three numerical methods in case $240°$ (left), $180°$ (center) and $\rho = 120°$ (right), while Figure 1 (bottom) shows their corresponding ARTs.

In our experiments, we generated the specified number of true points on the true ellipses. We then simulated $n = n_1 + n_2$ noisy values (δ_k, ϵ_k) from a normal distribution with mean zero and standard deviation σ and then they are added to the true points. Then three optimization algorithms were implemented and compared. Our numerical results are depicted in Figure 1. As shown in Figure 1, when $\rho = 240°$ the BFGS algorithm requires less time than the Nelder-Mead and L-BFGS-B algorithms for each value of σ. In addition, we see that the BFGS and L-BFGS-B algorithms have coinciding divergence rates, being slightly lower than that of the Nelder-Mead algorithm. When $\rho = 180°$ the BFGS algorithm is faster than Nelder-Mead and has the lowest divergence rate. When $\rho = 120°$, on the other hand, the BFGS algorithm has a higher

ART as σ increases but has a lower divergence rate. Therefore, BFGS provides the best results and will be implemented in our second set of experiments.

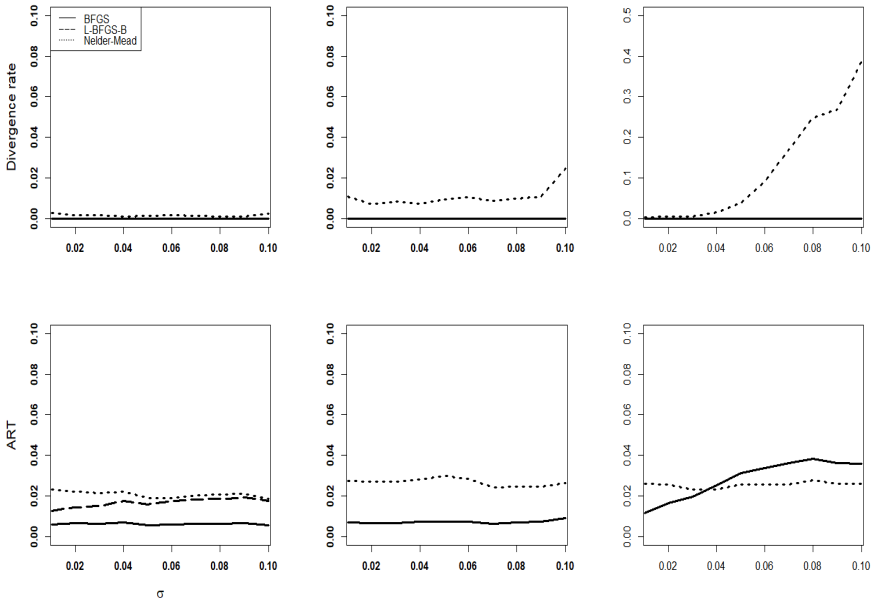

Fig. 1: (top) The divergence rate and (bottom) ART for the algorithms using the center averaging initial guess: BFGS (solid), Nelder-Mead (dotted), and L-BFGS-B (dashed). Here, $\rho = 240^\circ$, 180°, and 120°, respectively.

In the second set of experiments, we validate our theory through some Monte-Carlo simulations. We positioned $n_1 = 30$ and $n_2 = 45$ equidistant points that lie on the true ellipses and we considered the following true values of the parameters $x_c = 0$, $y_c = 0$, $b_1 = 1$, $a_2 = 3$, $b_2 = 2$, $\psi_1 = 0$, $\psi_2 = \frac{\pi}{4}$, while a_1 takes three values: $a_1 = 7$ (Figure 2 (top row)), $a_1 = 3$ (Figure 2 (middle row)), and $a_1 = 2$ (Figure 2 (bottom row)). The true points were distributed along arcs of circular angles 360° (left subfigures), 240° (centered subfigures), 180° (right subfigures). In each experiment, $N = 2000$ samples were generated by adding white noise of level σ to the true points and we computed the estimates of the LS and GRAF. Then we computed the *empirical normalized*

MSE ($\widehat{\text{NMSE}}$) of ϕ for each method and the normalized CCRB, i.e., $\frac{1}{\sigma^2}$CCRB, using $\widehat{\text{NMSE}}(\hat{\boldsymbol{\phi}}) = \frac{1}{N\sigma^2}\sum_{i=1}^{N}\|\hat{\boldsymbol{\phi}}_i - \tilde{\boldsymbol{\phi}}\|^2$, where $\frac{1}{\sigma^2}\text{CCRB} = \frac{1}{\sigma^2}\text{tr}\left((\tilde{\boldsymbol{Q}}_w^\top \tilde{\boldsymbol{Q}}_w)^{-1}\right)$, where $\hat{\boldsymbol{\phi}}_i$ is the i^{th} estimate of the true parameter vector $\tilde{\boldsymbol{\phi}}$. The dashed and the solid lines in Figure 2 represent $\widehat{\text{NMSE}}$ of the LS and GRAF, respectively, while the dotted line represents the normalized CCRB. We plotted the empirical NMSEs against σ. For smaller arc lengths, such as 180°, the two methods diverge faster, hence we computed the normalized MSE for σ up to .04 only as the figures on the right column reveal.

Our experiments show that GRAF estimator outperforms the LS estimator in terms of the empirical normalized MSE. For small values of σ, $\widehat{\text{NMSE}}(\hat{\boldsymbol{\phi}}_{\text{G}})$ approaches the CCRB regardless of the arc lengths, while $\widehat{\text{NMSE}}(\hat{\boldsymbol{\phi}}_{\text{L}})$ does not. This validates our theory in this paper. The differences between the normalized MSEs of the two methods increase as the arc length increases. Moreover, it is worth mentioning here that the normalized MSEs of the two methods become closer to the CCRB as a_1 decreases.

To corroborate our analytic findings with a set of practical data, we applied our algorithms to real images, and then we assessed their performances. Since one of the most important applications for fitting concentric ellipses appears in iris recognition Kong (2012); Pillai et al (2011) and astronomy, we applied all methods to the binary images of NGC 1415, which is a Lenticular Galaxy in the Eridanus constellation, and two images of human eye irises. In Figures 3–5, the LS and the GRAF methods were superimposed on the image. It is clear that the other approaches in concentric ellipses cannot be applied here. One can easily see that the LS and GRAF produce estimates that are very accurate in Figures 3 and 4. However, in a more challenging case presented in Figure 5, the LS produces heavy biased estimates of the fitted coupled ellipses, and as such, their estimates for the actual inner and outer boundaries

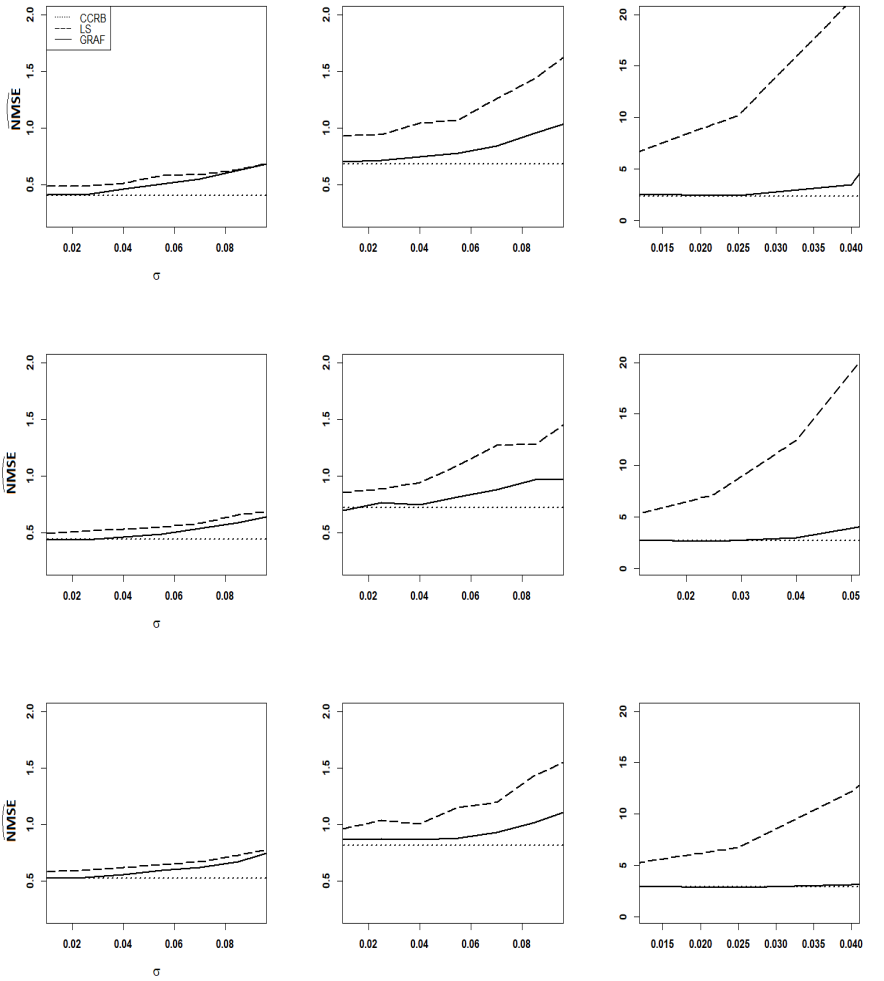

Fig. 2: The empirical NMSE for the LS (dashed) and GRAF (solid) versus σ. The normalized CCRB is given by the dotted line. The experiments are conducted for three values of arc degree: 360° (left), 240° (center), and 180° (right); while a_1 takes three values: 7 (top row), 3 (middle row), and 2 (bottom row).

are less satisfactory. This is not an unexpected observation regarding the LS method which is widely known to be heavily biased. This observation deserves a thorough theoretical investigation. On the other hand, the GRAF provides the closest fit to the inner ring of the iris.

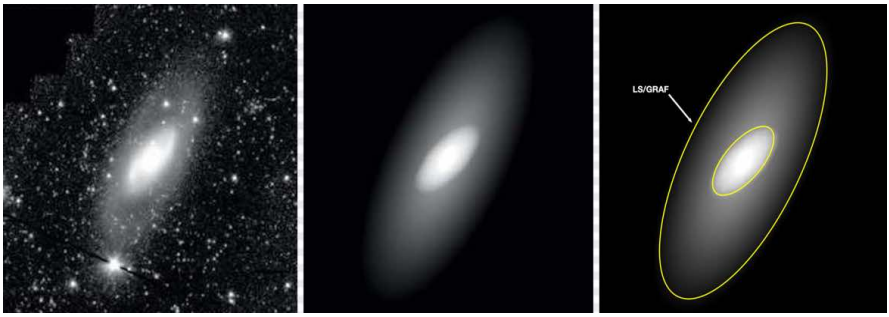

Fig. 3: The binary images of the Lenticular Galaxy NGC 1415 superimposed by the fitted methods.

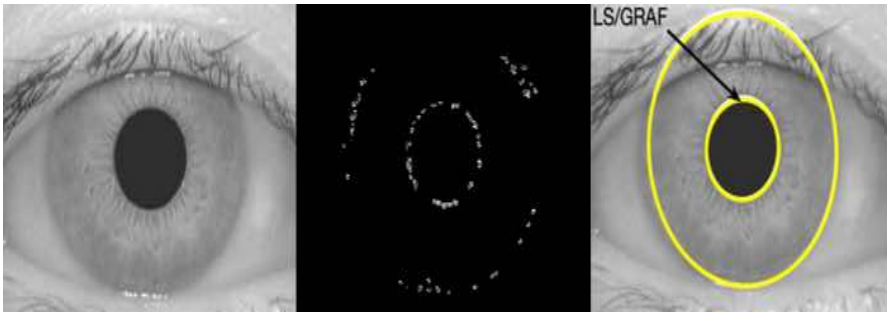

Fig. 4: The image of the eye's iris superimposed by the fitted methods.

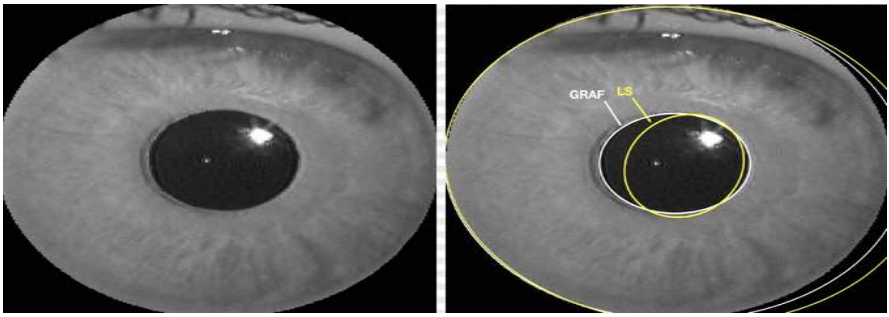

Fig. 5: The image of the eye's iris superimposed by the fitted methods.

References

Aggarwal CC (2018) Neural Networks and Deep Learning: A Textbook. Springer

Al-Sharadqah A, Chernov N (2012) A doubly optimal ellipse fit. Computational Statistics and Data Analysis 56:2771–2781

Al-Sharadqah A, Ho KC (2018) Constrained cramér-rao lower bound in errors-in variables (EIV) models: Revisited. Statistics & Probability Letters 35:118–126

Al-Sharadqah A, Rulli L (2022) New methods for detecting concentric objects with high accuracy. Measurement 188

Ambartsoumian G, Xie M (2010) Tomographic reconstruction of nodular images from incomplete data. AIP Conference Proceedings 1301(1):167 – 174

Amemiya Y, Fuller WA (1988) Estimation for the nonlinear functional relationship. Annals Statist 16:147–160

Bennamoun M, Mamic GJ (2002) Object recognition: Fundamentals and case studies. Springer-Verlag London

Chang L, Weiduo H (2019) Real-time geometric fitting and pose estimation for surface of revolution. Pattern Recognition 85:90–108

Chernov N, Lesort C (2004) Statistical efficiency of curve fitting algorithms. Comp Stat Data Anal 47:713–728

Kanatani K (1998) Cramér rao lower bounds for curve fitting. Graph Mod Image Process 60:93–99

Kanatani K (2008) Statistical optimization for geometric fitting: theoretical accuracy bound and high order error analysis. Int J Computer Vision 80:167–188

Kanatani K, Sugaya YY. ans Kanazawa (2016) Ellipse fitting for computer vision: Implementation and applications

Kilambi, Sreelatha, Tipton S (2011) Development of a laser scan inspection tool for coiled tubing. SPE/ICoTA Coiled Tubing & Well Intervention Conference and Exhibition

Kong AWK (2012) Iriscode decompression based on the dependence between its bit pairs. IEEE Trans, Pattern Anal Machine Intell 34(3):506–520

Kumar P, Belchamber ER, Miklavcic SJ (2018) Pre-processing by data augmentation for improved ellipse fitting. PLoS ONE 13(5)

Kunitomo N (1980) Asymptotic expansions of the distributions of estimators in a linear functional relationship and simultaneous equations. J Amer Statist Assoc 75:693–700

Kweon IS, Kim JS, Kim HW (2002) A camera calibration method using concentric circles of vision applications. In Asian Conf Comput Vision pp 512–520

M. Heidari PCH (1993) Determination of hydraulic conductivity tensor using a nonlinear least squares estimator. SWater Resour Bull

Mai F, Hung YS, Zhong H, et al (2008) A hierarchical approach for fast and robust ellipse extraction. Pattern Recognition 41

Pillai JK, Patel VM, R. Chellappa NKR (2011) Secure and robust iris recognition using random projections and sparse representations. IEEE Trans Pattern Anal Machine Intell 33:1877–1893

S. D. Connell AKJ (2001) Template based online character recognition

Salo H, et al (2014) Spitzer survey of stellar structure in galaxies. the pipeline 4: Multi-component decomposition strategies and data release. Astrophysical Journal Supplemental Series

Satriya T, Wibirama S, Ardiyanto I (2016) Robust pupil tracking algorithm based on ellipse fitting. 2016 ISESD Bandung, Indonesia pp 253–257

Stoica P, Ng B (1998) On the cramer-rao bound under parametric constraints. IEEE Signal Proc Lett 5(7):177–179

Taubin G (1991) Estimation of planar curves, surfaces and nonplanar space curves defined by implicit equations, with applications to edge and range image segmentation. IEEE Trans Pattern Analysis Machine Intelligence 13:1115–1138

Vincze M (2001) Robust tracking of ellipses at frame rate. Pattern Recognition 34:487

Zhao Y, Xiong C (2011) Prediction-based geometric feature extraction for 2d laser scanner. Robotics and Autonomous Systems 59(6):402–409